Biogeosciences

Supplement of

New insights into large-scale trends of apparent organic matter reactivity in marine sediments and patterns of benthic carbon transformation

Felipe S. Freitas et al.

Correspondence to: Felipe S. Freitas (felipe.salesdefreitas@bristol.ac.uk)

S1. Extended information on Study Sites

This section complements the information presented in Sect. 2 and Table 2 in the main manuscript. Table S1 displays further details on site descriptions regarding broad biological properties of each study site.

Table S1. Oceanographic and biologic context of depositional environments.

Site	Pelagic ecosystem structure	References
Severn estuary	Turbidity resulting from strong tidal dynamics restricts phytoplankton communities. In tidal flats microphytobenthos (mainly diatoms; but also, green algae, euglenophytes, and cyanobacteria) contributes to most of primary productivity.	Langston et al. (2010); Thomas (2014); Underwood (2010)
Rhone delta	Strong pulses of fresh water and sediments associated to flood events. Coccolithophorids are dominant year-round. During spring blooms, diatoms peak and dominates over cyanobacteria.	Antonelli et al. (2008); Cathalot et al. (2010); Zebracki et al. (2015); Uitz et al. (2012)
Aarhus Bay	Stable stratification separates upper oligotrophic wates from lower nutrient replete layers. Mixotrophic flagellates account for up to half of pigmented biomass in upper layers. Chl-a maxima develop at the pycnocline. Spring phytoplankton blooms dominated by diatoms.	Chen et al. (2017); Havskum and Riemann (1996); Jensen et al. (1990); Lomstein et al. (1990); Thingstad et al. (1996)
Arkona Basin	Long-term decrease in water transparency associated to eutrophication. Spring blooms are mainly dominated by diatoms and dinoflagellates. Cyanobacteria blooms occur in the end of summer.	Fleming and Kaitala (2006); Fleming-Lehtinen and Laamanen (2012); Zettler et al. (2007)
Helgoland Mud Area, North Sea	Spring blooms dominated by diatoms. Flagellates growth is restricted to summer months. Haptophytes represent a large contribution to phytoplankton community, although the timing and intensity of blooms vary in a less predictive way.	Hebbeln et al. (2003); Hickel et al. (1992); Riebesell (1993); Wiltshire and Manly (2004)
Skagerrak	Short-term and inter-annual variability in phytoplankton community is common. Chl-a displays a sub-surface maximum below pycnocline. Diatoms dominant during spring, whereas dinoflagellates are predominant during summer. Haptophytes account for half of nanophytoplankton. Cyanobacteria abundance is high in the central basin during summer.	Dahl and Johannessen (1998); Karlson et al. (1996); Richardson et al. (2003); Trimmer et al. (2013)
Arabian Sea	Monsoon regime drives hydrology and has a strong impact on the seasonality of primary productivity. Cyanobacteria dominates oligotrophic, warm upper waters. In subsurface waters eukaryotic phytoplankton are the dominant group and represents 50-80% of carbon biomass. Diatoms dominate coastal upwellings and are gradually replaced offshore by haptophytes.	Barlow et al. (1999); Cowie (2005); Latasa and Bidigare (1998); Rixen et al. (2019); Shalapyonok et al. (2001)
Bering Sea	Nutrient recycling and upwelling support autumn blooms. Ice melting triggers spring blooms. In the absence of sea ice, blooms are delayed until thermal stratification is established. Community composition is dominated by diatoms with small contribution of pico- and nanophytoplankton groups. Coccolithophores form large blooms during calm conditions.	Coyle et al. (2008); Gersonde (2009); Odate (1996); Stabeno and Hunt (2002); Stockwell et al. (2001)
Argentine Basin	Complex hydrology and water masses dynamics. Enhanced productivity at oceanographic fronts and Sub-Antarctic water upwellings. Haptophytes are the dominant group and dominant at shelf-break where strong mixing and nutrient renovation occur. Diatoms occur in low abundance. Other groups include pico-cyanobacteria, picoplanktonic coccoids, and flagellates.	Calliari et al. (2009); Carreto et al. (2003); Gayoso (1995); Peterson (1992)

S2. Extended information on Reaction-Transport Model description

The Biogeochemical Reaction Network Simulator (BRNS) (Aguilera et al., 2005; Regnier et al., 2002) is an adaptive simulation environment that has been successfully employed to reproduce and quantify diagenetic processes in marine sediments across a wide range of depositional environments and timescales (Thullner et al., 2009; Wehrmann et al., 2013). It calculates concentration depth profiles of solid and dissolved species in marine sediments according to the vertically-resolved mass conservation equation of solid and dissolved species in porous media (Berner, 1980; Boudreau, 1997):

$$\frac{\partial \sigma C_i}{\partial t} = \frac{\partial}{\partial z}\left(D_{bio}\sigma\frac{\partial C_i}{\partial z} + D_i\sigma\frac{\partial C_i}{\partial z}\right) - \frac{\partial \sigma \omega C_i}{\partial z} + \alpha_i\sigma(C_i(0) - C_i) + \sum_n s_i^n r_n$$

(S1)

The first three terms on the right-hand side represent the transport process (bioturbation and molecular diffusion, advection, and bioirrigation; see Sect. S2.1), whereas the last term denotes the sum of all reactions (production and consumption; see Sect. S2.2) that affect species i. Table S2 provides a summary of all symbols employed here. In the following sections, we provide a detailed description of the model parameterization and solution.

Table S2. Summary of model elements incorporated in the BRNS.

Symbol	Description
	Chemical species, i
TOC	Total organic carbon
CH_2O	Organic matter (simplified stoichiometry)
O_2	Oxygen
NO_3^-	Nitrate
SO_4^{2-}	Sulfate
CH_4	Methane
NH_4^+	Ammonium
PO_4^{3-}	Phosphate
HS^-	Sulfides
	Model parameters
C_i	Concentration of species i
t	Time
z	Sediment depth
L	Length of model domain
T	Temperature
S	Salinity
h	Water depth
	Porosity term
σ	Solid species, $\sigma = 1 - \varphi$
	Dissolved species, $\sigma = \varphi$
φ	Sediment porosity
φ_0	Porosity at sediment-water interface
φ_z	Porosity at depth
φ_∞	Porosity at greater depth
β	Porosity attenuation coefficient
ω	Burial velocity – sedimentation rates
ω_0	Burial velocity at sediment-water interface
ω_z	Burial velocity at depth
D_i	Effective molecular diffusion coefficient of dissolved species i at 0 °C
D_i^*	Corrected molecular diffusion coefficient of dissolved species i
D_{bio}	Bioturbation diffusion coefficient

z_{bio}	Depth of bioturbated zone – sediment mixed layer
α_i	Bioirrigation rate
α_0	Bioirrigation coefficient at sediment-water interface
x_{irri}	Bioirrigation attenuation depth length
s_i^n	Stoichiometric coefficient of specie i
n	Kinetically controlled reaction
r_n	Reaction rate
K_i	Half-saturation constant of species i
f_i	Primary redox reaction inhibition term of species i
k_n	First-order bimolecular rate constant of secondary redox reaction r_n
$x/y/z$	Stoichiometric constants
age	Age of organic matter
$\Gamma(v)$	gamma distribution
a	Reactive continuum model shaping parameter
v	Reactive continuum model scaling parameter
$om\,(k,t)$	Probability density function of OM distribution
G_i	Initial TOC proportion in fraction i – multi-G approximation of RCM
k_i	First-order degradation rate constant of fraction i
$g(k,0)$	Initial fraction of TOC characterized by a distinct reactivity
$G(k,0)$	Initial fraction of TOC within the reactivity range between 0 and k

S2.1. Transport parameters

The BRNS set-up used here accounts for sediment accumulation and compaction, molecular diffusion, bioturbation, and bioirrigation (see Eq. S1). Global transport parameter values are given in Table S3. Site-specific transport parameter values are given in the main manuscript (Table 5). Sediment porosity is assumed to decrease exponentially with depth due to sediment compaction:

$$\varphi_z = \varphi_\infty + (\varphi_0 - \varphi_\infty)exp(-\beta z) \tag{S2}$$

Consequently, the burial velocity is corrected for the effect of compaction assuming steady-state compaction (e.g., Berner, 1980):

$$\omega_z = \omega_0(1 - \varphi_0)/(1 - \varphi_z)$$
(S3)

The diffusive fluxes are commonly quantified by means of Fick's first law of diffusion, which depends on the molecular diffusive coefficient D_i (i = dissolved species) (Boudreau, 1997; Burdige, 2006). The effective molecular diffusion coefficients are derived from Van Cappelen and Wang (1996). Here, D_i are corrected for temperature, salinity, and tortuosity. For solid species $D_i = 0$, whereas for dissolved species the corrected D_i^* is given by Boudreau (1997):

$$D_i^* = \frac{D_i(T,S)}{1 - ln(\varphi^2)} \tag{S4}$$

The model also accounts for the effect of sediment reworking by infaunal organisms in the bioturbated upper sediment layer ($z < z_{bio}$). The process is generally described by a dispersive term with constant bioturbation

diffusion coefficient D_{bio} (Boudreau, 1986). For bioturbated sites, D_{bio} was constrained based on an empirically derived relationship proposed by Middelburg et al. (1997):

$$D_{bio} = 5.2 \cdot 10^{(0.7624 - 0.0003972 \cdot h)} \tag{S5}$$

For the Rhone delta, D_{bio} values were derived from Pastor et al. (2011). D_{bio} was kept constant within the bioturbated zone ($z < z_{bio}$) then set to zero below z_{bio}. Bioturbation depth was fixed at 10 cm for most bioturbated sediments (Table 4), based on a compilation of mixed layer depths (Boudreau, 1994, 1998). At anoxic depositional environments (i.e., where O_2 concentrations are zero), z_{bio} was set to zero (Table 4). Similarly, the bioturbation diffusion coefficient D_{bio} was set to zero in anoxic environments. Bioirrigation describes the mixing by benthic macrofaunal organisms that build burrows or tubes in the sediment for feeding. It is parameterized as a nonlocal transport process with a nonlocal bioirrigation coefficient α_i, which describes the exchange rates between the sediment-water interface and porewater at depth in bioirrigated zone of sediments (Aller, 1994; Aller and Aller, 1998; Burdige, 2006). The bioirrigation rate is given by (Thullner et al., 2009; Wehrmann et al., 2013):

$$\alpha_i = \alpha_0 \cdot exp(-x/x_{irri}) \tag{S6}$$

For solid species, α_i is set to zero.

Table S3. Global model transport parameter values implemented in the RTM. Effective molecular diffusion coefficients (D_i) are given for $T = 0$ °C and are corrected by site-specific temperature, salinity, and tortuosity.

Parameter	Unit	Value	Reference
α_0	yr^{-1}	10	Thullner et al. (2009)
x_{irri}	cm	3.5	Thullner et al. (2009)
D_{O_2}	cm^2 yr^{-1}	380.44	Van Cappellen and Wang (1996)
$D_{NO_3^-}$	cm^2 yr^{-1}	394.58	Van Cappellen and Wang (1996)
$D_{SO_4^{2-}}$	cm^2 yr^{-1}	173.92	Van Cappellen and Wang (1996)
$D_{NH_4^+}$	cm^2 yr^{-1}	395.87	Van Cappellen and Wang (1996)
D_{H_2S}	cm^2 yr^{-1}	331.61	Van Cappellen and Wang (1996)
$D_{CH_{4(g)}}$	cm^2 yr^{-1}	263.93	Van Cappellen and Wang (1996)

S2.2. Reaction parameters

The reaction network implemented in the BRNS encompasses the most pertinent primary and secondary redox reactions found in the upper layers of marine sediments. Its formulation and parametrization builds on a number of previous studies that investigate diagenetic dynamics across several depositional environments and scales (Aguilera et al., 2005; Thullner et al., 2009; Van Cappellen and Wang, 1996; Wang and Van Cappellen, 1996; Wehrmann et al., 2013). It explicitly accounts for the heterotrophic degradation of OM coupled to the consumption of oxygen (aerobic OM degradation), nitrate (denitrification), sulfate (organoclastic sulfate reduction), as well as methanogenesis. Additionally, it accounts for nitrification, sulfide re-oxidation by O_2, anaerobic oxidation of

methane (AOM) coupled to sulfate reduction and CH_4 reoxidation by O_2. Due to the limited availability of data to constrain manganese oxide (MnO_2) and iron hydroxide ($Fe(OH)_3$) depositional fluxes, the model does not account for metal oxides reduction pathways. At certain depositional settings (e.g., Skagerrak), metal oxide pathways can be relatively important (e.g., Canfield et al., 1993; Rysgaard et al., 2001), particularly in continental margins that receive considerable inputs of iron (Beckler et al., 2016). Nevertheless, a previously published global assessment of the importance of metabolic pathways in marine sediments has found their contributions to the overall heterotrophic OM degradation to be negligible at a global scale (Thullner et al., 2009).

Table S4. Reaction network governing heterotrophic organic matter degradation in marine sediments implemented in the Reaction-Transport Model (Adapted from Aguilera et al., 2005; Thullner et al., 2009; Wehrmann et al., 2013).

	Reaction Pathway	Stoichiometry	Reaction rate
		Primary redox reactions	
r_1	Aerobic OM degradation	$(CH_2O)_x(NH_3)_y(H_3PO_4)_z + (x+2y)O_2 + (y+2z)HCO_3^-$ $\rightarrow (x+y+2z)CO_2 + yNH_4^+ + zHPO_4^{2-}$ $+ (x+2y+2z)H_2O$	r_1 $= v \cdot (a+age)^{-1}$ $\cdot CH_2O \cdot f_{O_2}$
r_2	Denitrification	$(CH_2O)_x(NH_3)_y(H_3PO_4)_z + \left(\frac{4x+3y}{5}\right)NO_3^-$ $\rightarrow \left(\frac{2x+4y}{5}\right)N_2 + \left(\frac{x-3y+10z}{5}\right)CO_2$ $+ \left(\frac{4x+3y-10z}{5}\right)HCO_3^- + zPO_4^{2-}$ $+ \left(\frac{3x+6y+10z}{5}\right)H_2O$	r_2 $= v \cdot (a+age)^{-1}$ $\cdot CH_2O \cdot f_{NO_3}$
r_3	Sulfate reduction	$(CH_2O)_x(NH_3)_y(H_3PO_4)_z + \frac{x}{2}SO_4^{2-} + (y-2z)CO_2 + (y-2z)H_2O$ $\rightarrow (x+y-2z)HCO_3^- + yNH_4^+ + zHPO_4^{2-}$ $+ \frac{x}{2}H_2S$	r_3 $= v \cdot (a+age)^{-1}$ $\cdot CH_2O \cdot f_{SO_4^{2-}}$
r_4	Methanogenesis	$(CH_2O)_x(NH_3)_y(H_3PO_4)_z + (y-2z)H_2O$ $\rightarrow \left(\frac{x-2y+4z}{2}\right)CO_2 + (y-2z)HCO_3^- + yNH_4^+$ $+ zHPO_4^{2-} + \frac{x}{2}CH_4$	r_4 $= v \cdot (a+age)^{-1}$ $\cdot CH_2O \cdot f_{CH_4}$
		Secondary redox reactions	
r_5	Ammonium oxidation by oxygen	$NH_4^+ + 2O_2 + 2HCO_3^- \rightarrow NO_3^- + 2CO_2 + 3H_2O$	$r_5 = k_5 \cdot NH_4^+ \cdot O_2$
r_6	Sulfide oxidation by oxygen	$H_2S + 2O_2 + 2HCO_3^- \rightarrow SO_4^{2-} + 2CO_2 + 2H_2O$	$r_6 = k_6 \cdot (HS^- + H_2S)$ $\cdot O_2$
r_7	Anaerobic oxidation of methane (AOM)	$CH_4 + CO_2 + SO_4^{2-} \rightarrow 2HCO_3^- + H_2S$	$r_7 = k_7 \cdot CH_4 \cdot SO_4^{2-}$
r_8	Methane oxidation by oxygen	$CH_4 + 2O_2 \rightarrow CO_2 + 2H_2O$	$r_8 = k_8 \cdot CH_4 \cdot O_2$

OM heterotrophic degradation follows first-order degradation kinetics (see below; Sect. S2.3) and is coupled to the consumption of terminal electron acceptors (TEAs) (primary redox reactions, $r_1 - r_4$; Table S4). The

sequential utilization of TEAs is kinetically controlled by rate laws (Table S5) (e.g., Van Cappellen and Wang, 1996). Additionally, the reaction network accounts for the reoxidation of reduced species produced during OM heterotrophic degradation (secondary redox reactions; $r_5 - r_8$; Table S4). Following the classical approach, the rates of secondary redox reactions are described by bimolecular rate laws with the rate constant k_n (Van Cappellen and Wang, 1996). Global reaction parameter values are given in Table S6.

Table S5. Kinetic rate laws controlling the reaction network.

	Kinetic rate laws
r_1	$\begin{cases} f_{O_2} = 1 \text{ for } O_2 > K_{O_2} \\ f_{O_2} = \dfrac{O_2}{K_{O_2}} \text{ for } O_2 \leq K_{O_2} \end{cases}$
r_2	$\begin{cases} f_{NO_3^-} = 0 \text{ for } f_{O_2} = 1 \\ f_{NO_3^-} = \left(1 - f_{O_2}\right) \text{ for } f_{O_2} < 1 \text{ and } NO_3^- > K_{NO_3^-} \\ f_{NO_3^-} = \left(1 - f_{O_2}\right)\dfrac{NO_3^-}{K_{NO_3^-}} \text{ for } f_{O_2} < 1 \text{ and } NO_3^- \leq K_{NO_3^-} \end{cases}$
r_3	$\begin{cases} f_{SO_4^{2-}} = 0 \text{ for } f_{O_2} + f_{NO_3^-} = 1 \\ f_{SO_4^{2-}} = \left(1 - f_{NO_3}\right) \text{ for } f_{NO_3} < 1 \text{ and } SO_4^{2-} > K_{SO_4^{2-}} \\ f_{SO_4^{2-}} = \left(1 - f_{NO_3}\right)\dfrac{SO_4^{2-}}{K_{SO_4^{2-}}} \text{ for } f_{NO_3} < 1 \text{ and } SO_4^{2-} \leq K_{SO_4^{2-}} \end{cases}$
r_4	$f_{CH_4} = \left(1 - \left(f_{O_2} + f_{NO_3^-} + f_{SO_4^{2-}}\right)\right)$

Table S6. Global reaction parameter values implemented in the RTM.

Parameter	Unit	Value	Reference
$x/y/z$	–	106/16/1	Redfield (1934)
v	–	variable	Boudreau and Ruddick (1991)
a	yr	variable	Boudreau and Ruddick (1991)
age	yr	variable	Mogollón et al. (2012)
K_{O_2}	M	$8.0 \cdot 10^{-9}$	Van Cappellen and Wang (1996)
$K_{NO_3^-}$	M	$5.0 \cdot 10^{-9}$	Van Cappellen and Wang (1996)
$K_{SO_4^{2-}}$	M	$1.0 \cdot 10^{-7}$	Van Cappellen and Wang (1996)
k_5	$M^{-1} yr^{-1}$	$1.0 \cdot 10^7$	Dale et al. (2011)
k_6	$M^{-1} yr^{-1}$	$1.0 \cdot 10^9$	Dale et al. (2011)
k_7	$M^{-1} yr^{-1}$	$5.0 \cdot 10^6$	Dale et al. (2011)
k_8	$M^{-1} yr^{-1}$	$1.0 \cdot 10^{13}$	Dale et al. (2011)

S2.3 Organic matter degradation model

OM is composed of a complex and dynamic mixture of compounds that are distributed over a wide, continuous spectrum of reactivities. Thus, OM degradation is described by the reactive continuum model (RCM) (Boudreau and Ruddick, 1991), which assumes a continuous distribution of OM compounds over the entire reactivity spectrum. The RCM assumes that the initial distribution of OM compounds over the reactivity spectrum follows a gamma distribution that is completely determined by two free parameters: a is the average lifetime of the more reactive components of bulk OM, and v represents the dimensionless scaling parameter of the distribution near $k = 0$. As such, the RCM approach requires the definition of two parameters that will define the shape of the OM distribution over reactivity k:

$$k(z) = \frac{v}{a + age(z)} \tag{S7}$$

$age(z)$ denotes the age of the sediment layer at depth z. For non-bioturbated sediments ($z > z_{bio}$) the burial $age(z)$ can be calculated as a function of the burial velocity:

$$age(z) = age_0 + \frac{(1-\varphi)z + \beta^{-1}(\varphi_0 - \varphi_\infty)(exp(-\beta z) - 1)}{\omega(1 - \varphi_0)} \tag{S8}$$

However, within the bioturbated upper sediment layers, the age distribution of reactive species is controlled by both sedimentation, bioturbation, and the reactivity k of reactive species (Meile and Van Cappellen, 2005). As such, the RCM approach cannot easily be applied to the upper mixed sediment layers. Therefore, within the bioturbated layer ($z < z_{bio}$), the RCM is approximated by a discrete multi-G model (200 fractions) to circumvent the difficulty of quantifying OM ages within bioturbated sediments (Dale et al., 2015; Meile and Van Cappellen, 2005). The multi-G model approach divides the bulk OM into 200 discrete compound classes i each degrading according to first-order kinetics with a degradation rate constant k_i (Jørgensen, 1978). The degradation rate of the bulk OM, R_{TOC}, and the initial concentration of OM in compound class i, $TOC_i(0)$ are thus given by:

$$C_{ox}(z) = \sum_{i=1}^{200} k_i \cdot TOC_i(z) \tag{S9}$$

$$TOC_i(0) = G_i \cdot TOC \tag{S10}$$

The initial proportion of TOC in fraction i, G_i, as well as the compound class specific reactivity rate-constant k_i can be determined from the initial probability density function $om(k, t)$ that provides the concentration of TOC having a degradability k and $k + dk$ at time 0. The initial fraction of TOC characterized by a distinct reactivity k is given by $g(k, 0)$:

$$g(k, 0) = \frac{om(k, 0)}{TOC_0} = \frac{a^v \cdot k^{v-1} \cdot e^{-a \cdot k}}{\Gamma(v)} \tag{S11}$$

The initial fraction of TOC within the reactivity range between 0 and k is given by integrating Eq. S12 (if a, v, k > 0):

$$G(k, 0) = \int_0^k g(0, k)dk = \int_0^k \frac{a^v \cdot k^{v-1} \cdot e^{-a \cdot k}}{\Gamma(v)} dk = \left(\frac{1 - \Gamma(v, a \cdot k)}{\Gamma(v)} \right) \tag{S12}$$

Where $\Gamma(v, a \cdot k)$ denotes the inverse gamma distribution.

Within the bioturbated sediment layer, the RCM was approximated by dividing the reactivity range $k = [10^{-15}, 10^{(-\log(a)+2)}]$ into 200 equal reactivity bins, k_j. The initial fraction G_i of TOC within reactivity bin k_{j-1} and k_j (and thus with reactivity $k_i = k_{j-1} + \frac{k_j - k_{j-1}}{2}$) in the 200G-model is then calculated as:

$$G_i = G(k_j, 0) - G(k_{j-1}, 0) \tag{S13}$$

The least and the most reactive fractions G_1 and G_{200} with reactivity $k_1 = 10^{-15}$ yr^{-1} and $k_{200} = 10^{-\log(a)+2}$ yr^{-1}, respectively, are calculated based on the incomplete gamma distribution:

$$G_1 = \int_{k_1}^{\infty} g(k_1, 0)dk = \frac{\Gamma(v, a \cdot k_1)}{\Gamma(v)} \tag{S14}$$

$$G_{200} = \int_{k_{200}}^{\infty} g(k_{200}, 0)dk = \frac{\Gamma(v, a \cdot k_{200})}{\Gamma(v)} \tag{S15}$$

Once G_i and k_i are determined, the steady-state analytical solution of the diffusion-advection-reaction equation (Boudreau, 1997) for OM in the bioturbated zone can then be calculated by:

$$TOC(z) = \sum_{i=1}^{200} A_i \cdot \exp(a_i \cdot z) + B_i \cdot \exp(b_i \cdot z) \tag{S16}$$

with:

$$a_i = \frac{\omega - \sqrt{\omega^2 + 4 \cdot D_{bio} \cdot k_i}}{2 \cdot D_{bio}} \tag{S17}$$

and

$$b_i = \frac{\omega + \sqrt{\omega^2 + 4 \cdot D_{bio} \cdot k_i}}{2 \cdot D_{bio}} \tag{S18}$$

A_i and B_i denote integration constants that can be determined by defining appropriate boundary conditions (Boudreau, 1997) for OM at the upper and lower boundaries. Below the bioturbated zone, the depth evolution of TOC is determined by the RCM formulation.

S2.5 Model solution

Transport and reaction equations were solved sequentially. Firstly, the diffusion term was discretized at each time-step of the numerical integration using the semi-implicit Crank-Nicholson scheme. This was followed by the calculation of the advective transport, using a 3rd order accurate total variation diminishing algorithm with flux limiters (Regnier et al., 1998). The reaction network was subsequently solved. The mass-conservation equation (Eq. S1) was discretized on an uneven grid (Boudreau, 1997):

$$z(n) = \frac{L\left(\left(\xi_n^2 + \xi_c^2\right)^{0.5} - \xi_c\right)}{\left(L^2 + \xi_c^2\right)^{0.5} - \xi_c} \tag{S19}$$

where $z(n)$ is the depth of the nth grid point, L denotes the length of the model domain, ξ_n is a point in a hypothetical grid, and ξ_c is depth relative to which $z(n)$ is quadratically distributed for $\xi_n \gg \xi_n$ and linearly distributed for $\xi_n \ll \xi_n$. L and ξ_n were chosen so that the grid size, Δz, increases downcore from SWI to a maximum of L. The size of model domain L was fixed at 1,000 cm for all sites, except for the Bering Sea, in which the model domain is extended to 1,500 cm, due to the low sedimentation rate assumed for this site (Table 2). This choice is based on initial tests and ensures that the model domain covers the diagenetically most active zone, thus reducing the influence of biogeochemical dynamics in underlying sediments on biogeochemical dynamics within the model domain. BRNS was run until steady state ($\Delta t < 0.01$) was reached:

$$run\ time = 2 \cdot \frac{L}{\omega} \tag{S20}$$

S3. Establishing a minimum dataset of observations for the determination of apparent organic matter reactivity

We use an inverse model approach to extract the optimal OM reactivity parameter set a and v (i.e., the apparent OM reactivity) by assuming that the rank of a parameter set depends on the similarity between simulated and measured data. However, all inverse model approaches and, thus the quality of the inversely determined parameters are subject to limitations, such as core top loss, uniqueness of fit, unresolved processes, transient dynamics. These limitations can be alleviated by using comprehensive, multi-component observational data sets for the inverse modelling approach. However, especially on the global scale, data availability is often limited. Consequently, it is important to identify a minimum set of observational data that are widely available and comparably easy to measure. To identify such a minimum observational data set, we here tested performance of different artificial porewater data sets in determining apparent OM reactivity. Using an artificial dataset (Table S7; Fig. S1 and S2) that was generated by using a defined OM reactivity, we ran the inverse model approach (see main manuscript, Sect. 3.2.4) using 1) TOC profiles only and 2) TOC and SO_4^{2-} profiles.

Table S7. Model parameters and boundary conditions adopted in the sensitivity analyses used to determine the minimum dataset necessary to constrain apparent organic matter reactivity k based on the Reactive Continuum Model parameters a and v. Model parameters omitted here follow those in Tables S2 and S6.

Parameter	Unit	Value	Parameter	Unit	Value	Parameter	Unit	Value
Transport			*Reactions*			*Boundary conditions*		
L	cm	150	$x/y/z$	–	106/16/1	TOC	wt%	0.32
α_0	yr^{-1}	10	a	yr	$[10^{-3} - 10^7]$	O_2	μM	325
x_{irr}	cm	3.5	v	–	$[10^{-1} - 10^0]$	NO_3^-	μM	9
z_{bio}	cm	10				SO_4^{2-}	mM	28
D_{bio}	$cm^2\ yr^{-1}$	23.98				NH_4^+	μM	0
φ	–	0.47				HS^-	μM	0
ω	$cm\ yr^{-1}$	0.06				CH_4	μM	0
T	°C	0.65						
S	–	35						
h	m	250						

Our sensitivity analysis confirms that when TOC is considered as a single constraint, multiple pairs of a and v produce very similar TOC depth-profiles that fit the artificial data equally well (Fig. S1). Model results show that including SO_4^{2-} depth profiles add an additional constraint (Fig. S2) and facilitates the identification of a best fit a and v parameter set. This is illustrated by the Taylor diagrams (Taylor, 2001), which summarizes the statistical fitting (r, RMSD, and SD) (Fig. S3). In addition, because changes in a—v exert different effects on TOC and SO_4^{2-} depth profiles (Fig. S1 and S2), including these two species reduces the impact of the a—v correlation on the uniqueness of fit (Fig. S3).

CH_4 profiles potentially offer an additional qualitative constraint when the data are available. The dynamics of SO_4^{2-} and CH_4 are solely controlled by OM degradation and AOM (e.g., Bowles et al., 2014; Egger et al., 2018; Regnier et al., 2011), although their distributions can be also affected by bioirrigation in particularly shallow sulfate-methane transition zones (SMTZs) (e.g., Dale et al., 2019). In anoxic settings and deeply buried sediments, SO_4^{2-} is the dominant TEA and CH_4 is the most common reduced species (Jørgensen et al., 2019a, b). Thus, a combination of TOC, SO_4^{2-}, and CH_4 (if available to verify the depths of the SMTZ) depth profiles incorporate the information contained in the observed benthic sulfur and carbon dynamics and is sufficient to extract robust estimates of apparent OM reactivity and its evolution from the sediment-water interface down to the SMTZ.
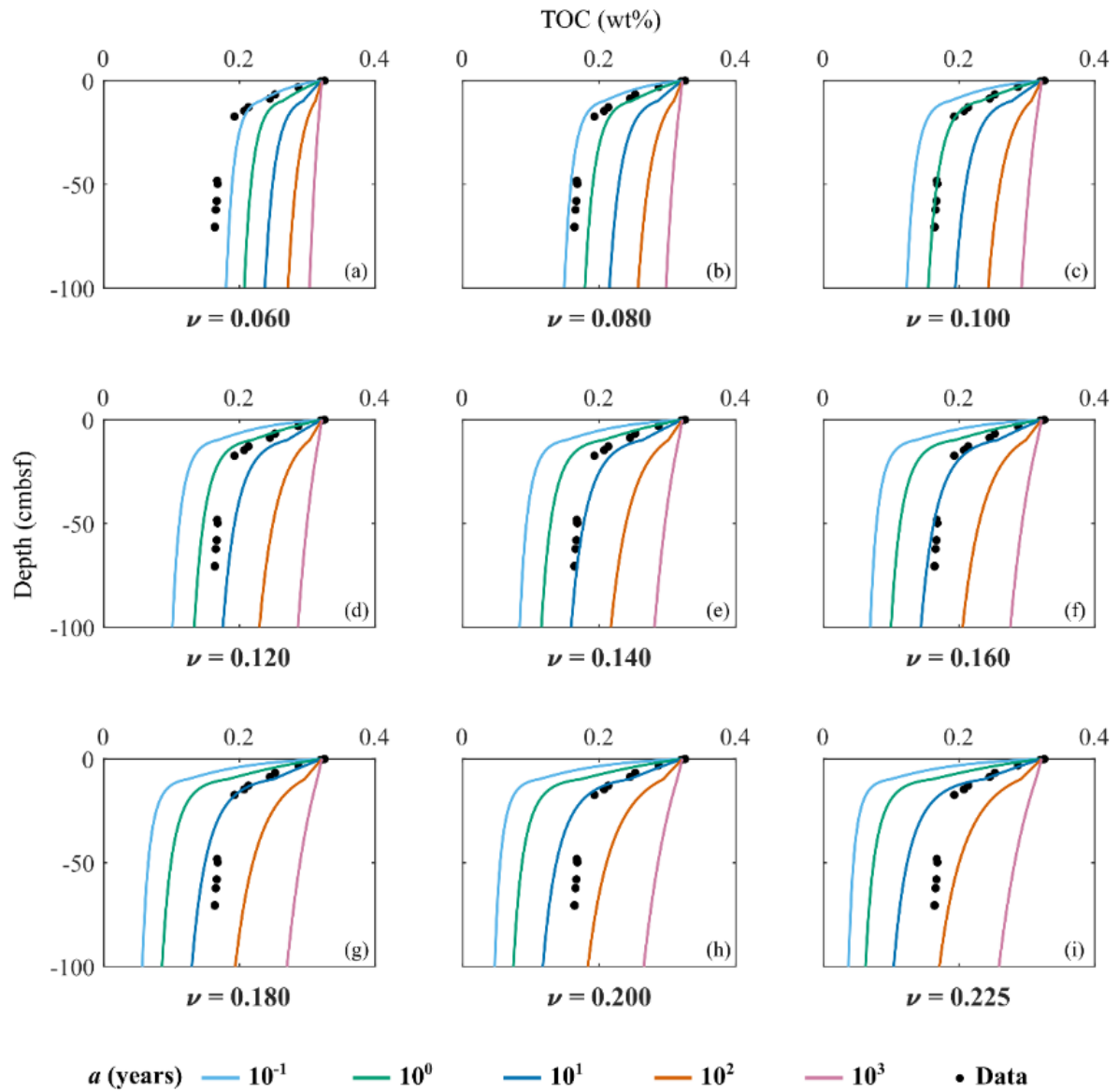
Figure S1. Total organic carbon depth profiles yielded by the sensitivity analysis for an ensemble of scaling parameter ν and shaping parameter a (see Table S3). Based on TOC alone multiple pairs of a and ν would be extracted from the same depth-profile.
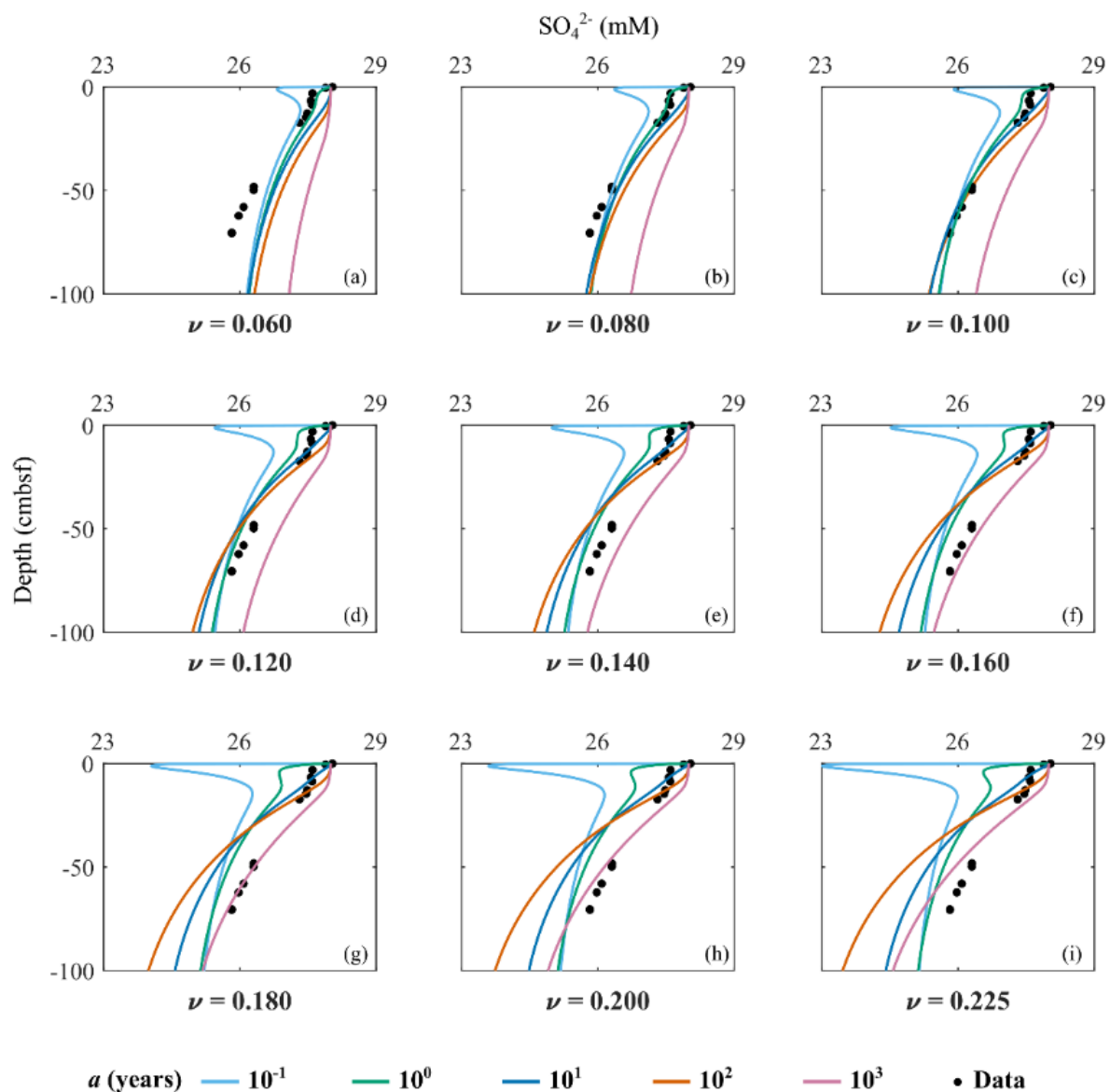
Figure S2. Sulfate depth profiles yielded by the sensitivity analysis for an ensemble of scaling parameter ν and shaping parameter a (see Table S3). Considering SO_4^{2-} alongside TOC improves the determination of a and ν by excluding those pairs that only fit TOC.
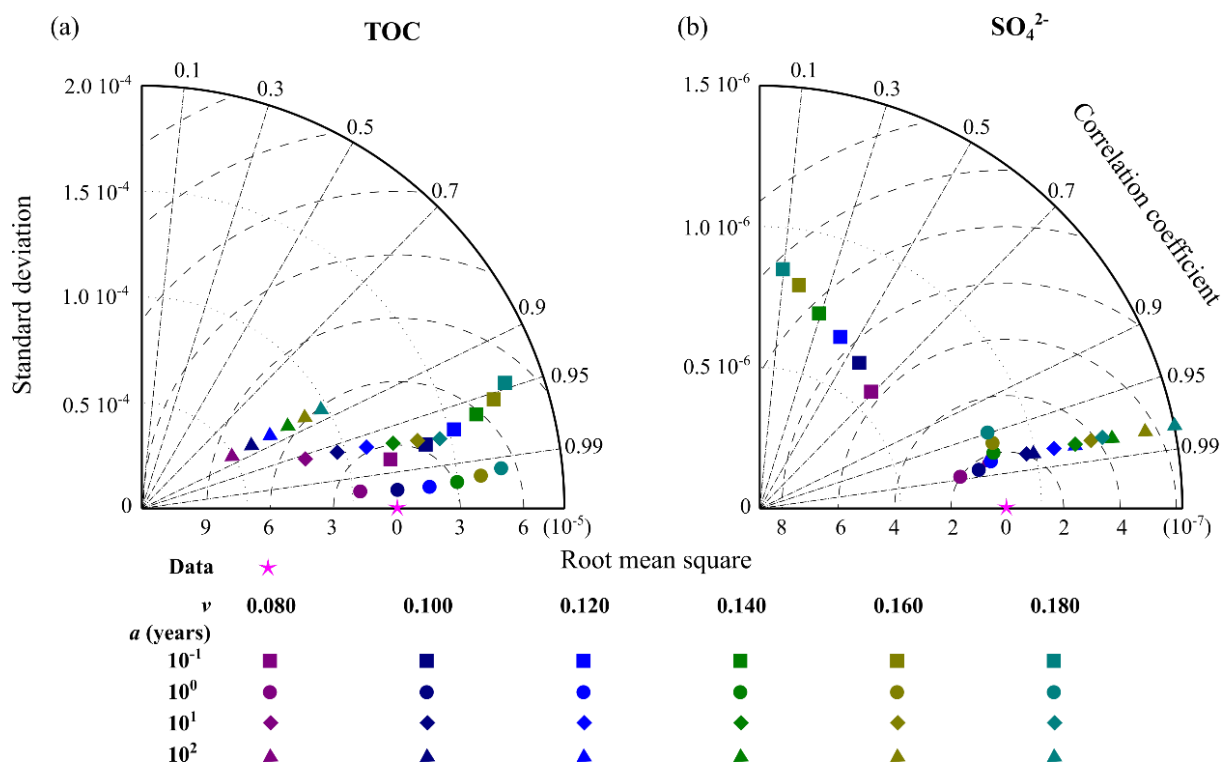
Figure S3. Sensitivity analysis best-fit based on Reactive Continuum model parameters a and v for (a) total organic carbon and (b) sulfate. The adoption of two species (i.e., TOC and SO_4^{2-}) relieves the uncertainties in constraining organic matter reactivity parameters.

References

Aguilera, D. R., Jourabchi, P., Spiteri, C., and Regnier, P.: A knowledge-based reactive transport approach for the simulation of biogeochemical dynamics in Earth systems, Geochem. Geophys. Geosystems, 6, 1–18, https://doi.org/10.1029/2004GC000899, 2005.

Aller, R. C.: Bioturbation and remineralization of sedimentary organic matter: effects of redox oscillation, Chem. Geol., 114, 331–345, https://doi.org/10.1016/0009-2541(94)90062-0, 1994.

Aller, R. C. and Aller, J. Y.: The effect of biogenic irrigation intensity and solute exchange on diagenetic reaction rates in marine sediments, J. Mar. Res., 56, 905–936, https://doi.org/10.1357/002224098321667413, 1998.

Antonelli, C., Eyrolle, F., Rolland, B., Provansal, M., and Sabatier, F.: Suspended sediment and 137Cs fluxes during the exceptional December 2003 flood in the Rhone River, southeast France, Geomorphology, 95, 350–360, https://doi.org/10.1016/j.geomorph.2007.06.007, 2008.

Barlow, R. G., Mantoura, R. F. C., and Cummings, D. G.: Monsoonal influence on the distribution of phytoplankton pigments in the Arabian Sea, Deep Sea Res. Part II Top. Stud. Oceanogr., 46, 677–699, https://doi.org/10.1016/S0967-0645(98)00123-4, 1999.

Beckler, J. S., Kiriazis, N., Rabouille, C., Stewart, F. J., and Taillefert, M.: Importance of microbial iron reduction in deep sediments of river-dominated continental-margins, Mar. Chem., 178, 22–34, https://doi.org/10.1016/j.marchem.2015.12.003, 2016.

Berner, R. A.: Early diagenesis: a theoretical approach, Princeton University Press, Princeton, N.J, 241 pp., 1980.

Boudreau, B. P.: Mathematics of tracer mixing in sediments; II, Nonlocal mixing and biological conveyor-belt phenomena, Am. J. Sci., 286, 199–238, https://doi.org/10.2475/ajs.286.3.199, 1986.

Boudreau, B. P.: Is burial velocity a master parameter for bioturbation?, Geochim. Cosmochim. Acta, 58, 1243–1249, https://doi.org/10.1016/0016-7037(94)90378-6, 1994.

Boudreau, B. P.: Diagenetic Models and Their Implementation: Modelling Transport and Reactions in Aquatic Sediments, Springer Berlin Heidelberg, Berlin, Heidelberg, 1997.

Boudreau, B. P.: Mean mixed depth of sediments: The wherefore and the why, Limnol. Oceanogr., 43, 524–526, https://doi.org/10.4319/lo.1998.43.3.0524, 1998.

Boudreau, B. P. and Ruddick, B. R.: On a reactive continuum representation of organic matter diagenesis, Am. J. Sci., 291, 507–538, https://doi.org/10.2475/ajs.291.5.507, 1991.

Bowles, M. W., Mogollon, J. M., Kasten, S., Zabel, M., and Hinrichs, K.-U.: Global rates of marine sulfate reduction and implications for sub-sea-floor metabolic activities, Science, 344, 889–891, https://doi.org/10.1126/science.1249213, 2014.

Burdige, D. J.: Geochemistry of marine sediments, Princeton University Press, Princeton, NJ, 609 pp., 2006.

Calliari, D., Brugnoli, E., Ferrari, G., and Vizziano, D.: Phytoplankton distribution and production along a wide environmental gradient in the South-West Atlantic off Uruguay, Hydrobiologia, 620, 47–61, https://doi.org/10.1007/s10750-008-9614-7, 2009.

Canfield, D. E., Jørgensen, B. B., Fossing, H., Glud, R., Gundersen, J., Ramsing, N. B., Thamdrup, B., Hansen, J. W., Nielsen, L. P., and Hall, P. O. J.: Pathways of organic carbon oxidation in three continental margin sediments, Mar. Geol., 113, 27–40, https://doi.org/10.1016/0025-3227(93)90147-N, 1993.

Carreto, J. I., Montoya, N. G., Benavides, H. R., Guerrero, R., and Carignan, M. O.: Characterization of spring phytoplankton communities in the Rio de La Plata maritime front using pigment signatures and cell microscopy, Mar. Biol., 143, 1013–1027, https://doi.org/10.1007/s00227-003-1147-z, 2003.

Cathalot, C., Rabouille, C., Pastor, L., Deflandre, B., Viollier, E., Buscail, R., Grémare, A., Treignier, C., and Pruski, A.: Temporal variability of carbon recycling in coastal sediments influenced by rivers: assessing the impact of flood inputs in the Rhône River prodelta, Biogeosciences, 7, 1187–1205, https://doi.org/10.5194/bg-7-1187-2010, 2010.

Chen, X., Andersen, T. J., Morono, Y., Inagaki, F., Jørgensen, B. B., and Lever, M. A.: Bioturbation as a key driver behind the dominance of Bacteria over Archaea in near-surface sediment, Sci. Rep., 7, 2400, https://doi.org/10.1038/s41598-017-02295-x, 2017.

Cowie, G.: The biogeochemistry of Arabian Sea surficial sediments: A review of recent studies, Prog. Oceanogr., 65, 260–289, https://doi.org/10.1016/j.pocean.2005.03.003, 2005.

Coyle, K. O., Pinchuk, A. I., Eisner, L. B., and Napp, J. M.: Zooplankton species composition, abundance and biomass on the eastern Bering Sea shelf during summer: The potential role of water-column stability and nutrients in structuring the zooplankton community, Deep Sea Res. Part II Top. Stud. Oceanogr., 55, 1775–1791, https://doi.org/10.1016/j.dsr2.2008.04.029, 2008.

Dahl, E. and Johannessen, T.: Temporal and spatial variability of phytoplankton and chlorophyll a: lessons from the south coast of Norway and the Skagerrak, ICES J. Mar. Sci., 55, 680–687, https://doi.org/10.1006/jmsc.1998.0401, 1998.

Dale, A. W., Regnier, P., Knab, N. J., Jørgensen, B. B., and Van Cappellen, P.: Anaerobic oxidation of methane (AOM) in marine sediments from the Skagerrak (Denmark): II. Reaction-transport modeling, Geochim. Cosmochim. Acta, 72, 2880–2894, https://doi.org/10.1016/j.gca.2007.11.039, 2008.

Dale, A. W., Sommer, S., Bohlen, L., Treude, T., Bertics, V. J., Bange, H. W., Pfannkuche, O., Schorp, T., Mattsdotter, M., and Wallmann, K.: Rates and regulation of nitrogen cycling in seasonally hypoxic sediments during winter (Boknis Eck, SW Baltic Sea): Sensitivity to environmental variables, Estuar. Coast. Shelf Sci., 95, 14–28, https://doi.org/10.1016/j.ecss.2011.05.016, 2011.

Dale, A. W., Nickelsen, L., Scholz, F., Hensen, C., Oschlies, A., and Wallmann, K.: A revised global estimate of dissolved iron fluxes from marine sediments, Glob. Biogeochem. Cycles, 29, 691–707, https://doi.org/10.1002/2014GB005017, 2015.

Dale, A. W., Flury, S., Fossing, H., Regnier, P., Røy, H., Scholze, C., and Jørgensen, B. B.: Kinetics of organic carbon mineralization and methane formation in marine sediments (Aarhus Bay, Denmark), Geochim. Cosmochim. Acta, 252, 159–178, https://doi.org/10.1016/j.gca.2019.02.033, 2019.

Egger, M., Riedinger, N., Mogollón, J. M., and Jørgensen, B. B.: Global diffusive fluxes of methane in marine sediments, Nat. Geosci., 11, 421–425, https://doi.org/10.1038/s41561-018-0122-8, 2018.

Fleming, V. and Kaitala, S.: Phytoplankton Spring Bloom Intensity Index for the Baltic Sea Estimated for the years 1992 to 2004, Hydrobiologia, 554, 57–65, https://doi.org/10.1007/s10750-005-1006-7, 2006.

Fleming-Lehtinen, V. and Laamanen, M.: Long-term changes in Secchi depth and the role of phytoplankton in explaining light attenuation in the Baltic Sea, Estuar. Coast. Shelf Sci., 102–103, 1–10, https://doi.org/10.1016/j.ecss.2012.02.015, 2012.

Gayoso, A. M.: Bloom of Emiliania huxleyi (Prymnesiophyceae) in the western South Atlantic Ocean, J. Plankton Res., 17, 1717–1722, https://doi.org/10.1093/plankt/17.8.1717, 1995.

Gersonde, R.: The expedition of the research vessel "Sonne" to the subpolar North Pacific and the Bering Sea in 2009 (SO202-INOPEX) (Reports on polar and marine research No. 643), Alfred Wegener Institute for Polar and Marine Research, Bremerhaven, 2009.

Havskum, H. and Riemann, B.: Ecological importance of bacterivorous, pigmented flagellates (mixotrophs) in the Bay of Aarhus, Denmark, Mar. Ecol. Prog. Ser., 137, 251–263, https://doi.org/10.3354/meps137251, 1996.

Hebbeln, D., Scheurle, C., and Lamy, F.: Depositional history of the Helgoland mud area, German Bight, North Sea, Geo-Mar. Lett., 23, 81–90, https://doi.org/10.1007/s00367-003-0127-0, 2003.

Hensen, C., Zabel, M., Pfeifer, K., Schwenk, T., Kasten, S., Riedinger, N., Schulz, H. D., and Boetius, A.: Control of sulfate pore-water profiles by sedimentary events and the significance of anaerobic oxidation of methane for the burial of sulfur in marine sediments, Geochim. Cosmochim. Acta, 67, 2631–2647, https://doi.org/10.1016/S0016-7037(03)00199-6, 2003.

Hickel, W., Berg, J., and Treutner, K.: Variability in phytoplankton biomass in the German Bight near Helgoland, in: ICES Mar Sci Symp, 249–259, 1992.

Hilligsøe, K. M., Jensen, J. B., Ferdelman, T. G., Fossing, H., Lapham, L., Røy, H., and Jørgensen, B. B.: Methane fluxes in marine sediments quantified through core analyses and seismo-acoustic mapping (Bornholm Basin, Baltic Sea), Geochim. Cosmochim. Acta, 239, 255–274, https://doi.org/10.1016/j.gca.2018.07.040, 2018.

Jensen, M., Lomstein, E., and Sørensen, J.: Benthic NH_4+ and NO_3- flux following sedimentation of a spring phytoplankton bloom in Aarhus Bight, Denmark, Mar. Ecol. Prog. Ser., 61, 87–96, https://doi.org/10.3354/meps061087, 1990.

Jørgensen, B. B.: A comparison of methods for the quantification of bacterial sulfate reduction in coastal marine sediments: II. Calculation from mathematical models, Geomicrobiol. J., 1, 29–47, https://doi.org/10.1080/01490457809377722, 1978.

Jørgensen, B. B., Beulig, F., Egger, M., Petro, C., Scholze, C., and Røy, H.: Organoclastic sulfate reduction in the sulfate-methane transition of marine sediments, Geochim. Cosmochim. Acta, 254, 231–245, https://doi.org/10.1016/j.gca.2019.03.016, 2019a.

Jørgensen, B. B., Findlay, A. J., and Pellerin, A.: The Biogeochemical Sulfur Cycle of Marine Sediments, Front. Microbiol., 10, 849, https://doi.org/10.3389/fmicb.2019.00849, 2019b.

Karlson, B., Edler, L., Granéli, W., Sahlsten, E., and Kuylenstierna, M.: Subsurface chlorophyll maxima in the Skagerrak-processes and plankton community structure, J. Sea Res., 35, 139–158, https://doi.org/10.1016/S1385-1101(96)90742-X, 1996.

Langston, W. J., Pope, N. D., Jonas, P. J. C., Nikitic, C., Field, M. D. R., Dowell, B., Shillabeer, N., Swarbrick, R. H., and Brown, A. R.: Contaminants in fine sediments and their consequences for biota of the Severn Estuary, Mar. Pollut. Bull., 61, 68–82, https://doi.org/10.1016/j.marpolbul.2009.12.014, 2010.

Latasa, M. and Bidigare, R. R.: A comparison of phytoplankton populations of the Arabian Sea during the Spring Intermonsoon and Southwest Monsoon of 1995 as described by HPLC-analyzed pigments, Deep Sea Res. Part II Top. Stud. Oceanogr., 45, 2133–2170, https://doi.org/10.1016/S0967-0645(98)00066-6, 1998.

Lomstein, E., Jensen, M. H., and Sørensen, J.: Intracellular NH_4+ and NO_3- pools associated with deposited phytoplankton in a marine sediment (Aarhus Bight, Denmark), Mar. Ecol. Prog. Ser., 61, 97–105, 1990.

Meile, C. and Van Cappellen, P.: Particle age distributions and O_2 exposure times: Timescales in bioturbated sediments, Glob. Biogeochem. Cycles, 19, 1–12, https://doi.org/10.1029/2004GB002371, 2005.

Middelburg, J. J., Soetaert, K., and Herman, P. M. J.: Empirical relationships for use in global diagenetic models, Deep Sea Res. Part Oceanogr. Res. Pap., 44, 327–344, https://doi.org/10.1016/S0967-0637(96)00101-X, 1997.

Mogollón, J. M., Dale, A. W., Fossing, H., and Regnier, P.: Timescales for the development of methanogenesis and free gas layers in recently-deposited sediments of Arkona Basin (Baltic Sea), Biogeosciences, 9, 1915–1933, https://doi.org/10.5194/bg-9-1915-2012, 2012.

Odate, T.: Abundance and size composition of the summer phytoplankton communities in the western North Pacific Ocean, the Bering Sea, and the Gulf of Alaska, J. Oceanogr., 52, 335–351, https://doi.org/10.1007/BF02235928, 1996.

Pastor, L., Deflandre, B., Viollier, E., Cathalot, C., Metzger, E., Rabouille, C., Escoubeyrou, K., Lloret, E., Pruski, A. M., Vétion, G., Desmalades, M., Buscail, R., and Grémare, A.: Influence of the organic matter composition on benthic oxygen demand in the Rhône River prodelta (NW Mediterranean Sea), Cont. Shelf Res., 31, 1008–1019, https://doi.org/10.1016/j.csr.2011.03.007, 2011.

Peterson, R. G.: The boundary currents in the western Argentine Basin, Deep Sea Res. Part Oceanogr. Res. Pap., 39, 623–644, https://doi.org/10.1016/0198-0149(92)90092-8, 1992.

Redfield, A. C.: On the proportions of organic derivatives in sea water and their relation to the composition of plankton, in: James Johnstone Memorial Volume, University Press of Liverpool, 176–192, 1934.

Regnier, P., Mouchet, A., Wollast, R., and Ronday, F.: A discussion of methods for estimating residual fluxes in strong tidal estuaries, Cont. Shelf Res., 18, 1543–1571, https://doi.org/10.1016/S0278-4343(98)00071-5, 1998.

Regnier, P., O'Kane, J. P., Steefel, C. I., and Vanderborght, J. P.: Modeling complex multi-component reactive-transport systems: towards a simulation environment based on the concept of a Knowledge Base, Appl. Math. Model., 26, 913–927, https://doi.org/10.1016/S0307-904X(02)00047-1, 2002.

Regnier, P., Dale, A. W., Arndt, S., LaRowe, D. E., Mogollón, J., and Van Cappellen, P.: Quantitative analysis of anaerobic oxidation of methane (AOM) in marine sediments: A modeling perspective, Earth-Sci. Rev., 106, 105–130, https://doi.org/10.1016/j.earscirev.2011.01.002, 2011.

Richardson, K., Rasmussen, B., Bunk, T., and Mouritsen, L. T.: Multiple subsurface phytoplankton blooms occurring simultaneously in the Skagerrak, J. Plankton Res., 25, 799–813, https://doi.org/10.1093/plankt/25.7.799, 2003.

Riebesell, U.: Aggregation of Phaeocystis during phytoplankton spring blooms in the southern North Sea, Mar. Ecol. Prog. Ser., 96, 281–289, 1993.

Rixen, T., Gaye, B., and Emeis, K.-C.: The monsoon, carbon fluxes, and the organic carbon pump in the northern Indian Ocean, Prog. Oceanogr., 175, 24–39, https://doi.org/10.1016/j.pocean.2019.03.001, 2019.

Rysgaard, S., Fossing, H., and Jensen, M. M.: Organic matter degradation through oxygen respiration, denitrification, and manganese, iron, and sulfate reduction in marine sediments (the Kattegat and the Skagerrak), Ophelia, 55, 77–91, https://doi.org/10.1080/00785236.2001.10409475, 2001.

Shalapyonok, A., Olson, R. J., and Shalapyonok, L. S.: Arabian Sea phytoplankton during Southwest and Northeast Monsoons 1995: composition, size structure and biomass from individual cell properties measured by flow cytometry, Deep Sea Res. Part II Top. Stud. Oceanogr., 48, 1231–1261, https://doi.org/10.1016/S0967-0645(00)00137-5, 2001.

Stabeno, P. J. and Hunt, G. L.: Overview of the Inner Front and Southeast Bering Sea Carrying Capacity Programs, Deep Sea Res. Part II Top. Stud. Oceanogr., 49, 6157–6168, https://doi.org/10.1016/S0967-0645(02)00339-9, 2002.

Stockwell, D. A., Whitledge, T. E., Zeeman, S. I., Coyle, K. O., Napp, J. M., Brodeur, R. D., Pinchuk, A. I., and Hunt, G. L.: Anomalous conditions in the south-eastern Bering Sea, 1997: nutrients, phytoplankton and zooplankton, Fish. Oceanogr., 10, 99–116, https://doi.org/10.1046/j.1365-2419.2001.00158.x, 2001.

Taylor, K. E.: Summarizing multiple aspects of model performance in a single diagram, J. Geophys. Res. Atmospheres, 106, 7183–7192, https://doi.org/10.1029/2000JD900719, 2001.

Thingstad, T. F., Riemann, B., Havskum, H., and Garde, K.: Incorporation rates and biomass content of C and P in phytoplankton and bacteria in the Bay of Aarhus (Denmark) June 1992, J. Plankton Res., 18, 97–121, https://doi.org/10.1093/plankt/18.1.97, 1996.

Thomas, S.: The response of anaerobic prokaryotic processes and communities in the Severn Estuary sediments to environmental changes, Cardiff University, Cardiff, 2014.

Thullner, M., Dale, A. W., and Regnier, P.: Global-scale quantification of mineralization pathways in marine sediments: A reaction-transport modeling approach, Geochem. Geophys. Geosystems, 10, 1–24, https://doi.org/10.1029/2009GC002484, 2009.

Trimmer, M., Engström, P., and Thamdrup, B.: Stark Contrast in Denitrification and Anammox across the Deep Norwegian Trench in the Skagerrak, Appl. Environ. Microbiol., 79, 7381–7389, https://doi.org/10.1128/AEM.01970-13, 2013.

Uitz, J., Stramski, D., Gentili, B., D'Ortenzio, F., and Claustre, H.: Estimates of phytoplankton class-specific and total primary production in the Mediterranean Sea from satellite ocean color observations, Glob. Biogeochem. Cycles, 26, 1–10, https://doi.org/10.1029/2011GB004055, 2012.

Underwood, G. J. C.: Microphytobenthos and phytoplankton in the Severn estuary, UK: Present situation and possible consequences of a tidal energy barrage, Mar. Pollut. Bull., 61, 83–91, https://doi.org/10.1016/j.marpolbul.2009.12.015, 2010.

Van Cappellen, P. and Wang, Y.: Cycling of iron and manganese in surface sediments; a general theory for the coupled transport and reaction of carbon, oxygen, nitrogen, sulfur, iron, and manganese, Am. J. Sci., 296, 197–243, https://doi.org/10.2475/ajs.296.3.197, 1996.

Wang, Y. and Van Cappellen, P.: A multicomponent reactive transport model of early diagenesis: Application to redox cycling in coastal marine sediments, Geochim. Cosmochim. Acta, 60, 2993–3014, https://doi.org/10.1016/0016-7037(96)00140-8, 1996.

Wehrmann, L. M., Arndt, S., März, C., Ferdelman, T. G., and Brunner, B.: The evolution of early diagenetic signals in Bering Sea subseafloor sediments in response to varying organic carbon deposition over the last 4.3Ma, Geochim. Cosmochim. Acta, 109, 175–196, https://doi.org/10.1016/j.gca.2013.01.025, 2013.

Wiltshire, K. H. and Manly, B. F. J.: The warming trend at Helgoland Roads, North Sea: phytoplankton response, Helgol. Mar. Res., 58, 269–273, https://doi.org/10.1007/s10152-004-0196-0, 2004.

Zebracki, M., Eyrolle-Boyer, F., Evrard, O., Claval, D., Mourier, B., Gairoard, S., Cagnat, X., and Antonelli, C.: Tracing the origin of suspended sediment in a large Mediterranean river by combining continuous river monitoring and measurement of artificial and natural radionuclides, Sci. Total Environ., 502, 122–132, https://doi.org/10.1016/j.scitotenv.2014.08.082, 2015.

Zettler, M. L., Schiedek, D., and Bobertz, B.: Benthic biodiversity indices versus salinity gradient in the southern Baltic Sea, Mar. Pollut. Bull., 55, 258–270, https://doi.org/10.1016/j.marpolbul.2006.08.024, 2007.